SAS v5.0 Scientific Validation report

Observation 0123700101 - Revolution 70 - Lockman Hole

M.Guainazzi[1], C.Gabriel[1], J.Osborne[2], M.Ehle[1], A.Talavera[1], B.Altieri[1]

[1] *XMM-Newton Science Operation Center, VILSPA, ESA, Apartado 50727, E-28080 Madrid, Spain*
[2] *XMM-Newton Science Survey Center, Department of Physics & Astronomy, University of Leicester, Leicester LE1 7RH, UK*

27 December 2000

We report the results of the scientific validation of the XMM-Newton Science Analysis System (SAS) version 5.0 (SASv5 hereinafter), performed on the data of observation nr.**0123700101**. These data belong to the XMM-Newton Performance Verification (PV) phase. They are free from data rights.

The reader is referred to the available documentation for a general description of the SAS, of the XMM-Newton data (Observation Data File, ODF), and of the PPS (Processing Pipeline Subsystem; "pipeline" hereinafter) products:

- "User's Guide of the XMM-Newton Science Analysis System", available at `http://xmm.vilspa.esa.es/sas/xmmsas_20001215_0000/htmldoc/doc/userguide/index.html` (SAS UH hereinafter)
- "XMM-Newton Data Files Handbook", available at `http://xmm.vilspa.esa.es/sas/xmmsas_20001215_0000/htmldoc/doc/dfh.ps.gz`

More information can be found, browsing the on-line SAS pages. The top browsing URL is: `http://xmm.vilspa.esa.es/user/sas_top.html`.

1 Purpose of the observation and instrument modes

XMM-Newton observed the region known as "Lockman Hole" (LH; α_{2000}=$10^h52^m43^s.0$, δ_{2000}=+57°28'.48".0) on April 27 2000, between 02:45:02 and 22:07:43 UTC (revolution number 70). Hasinger et al. (2001) have published preliminary scientific results of this observation.

The purpose of including this observation in the SAS science validation process was mainly to:

- check the basic SAS functionalities on EPIC data in Full Frame mode
- verify the accuracy of the XMM-Newton astrometry
- check the performances of the sources detection interactive pipeline (aka `edetectproc`)

The observation was affected by high level of radiation during its last 15 ks. In Fig. 1 we show a MOS image and light curve of the whole LH field of view in the 0.5–10 keV energy band, which clearly show the effect of the high radiation interval.

The instrument modes used in the *scheduled* observation (see Sect. 2.1) are listed in Tab. 1

2 Pipeline products

SAS tasks used to run the pipeline were all those included in SASv5, except:

- `ppssumm`
- `obssumm (4.1.2)`
- `dpsssrc`
- `implot (1.3.2)`
- `eexpmap (3.6.1)`

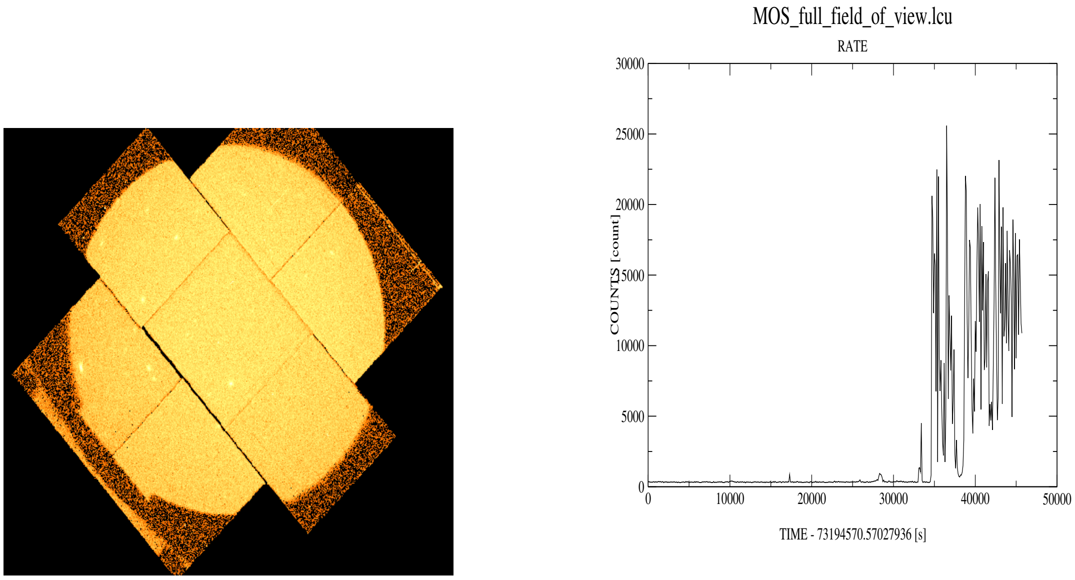

Figure 1: *Left panel*: MOS image in the 0.5-10 keV energy band. *Right panel*: MOS light curve of the whole field of view. The effect of the high radiation level in the last 15 ks of the observation is evident

Instrument	Exposure	Mode	Filter
MOS1	1	Full Frame	Thin
MOS2	2	Full Frame	Thin
p-n	3	Full Frame	Thin
RGS1	16	Spectroscopy+Q	
	18	HER+SES	
RGS2	17	Spectroscopy+Q	
	18	HER+SES	
OM	4	Image	V
	5	Image	U no barred
	6	Image	White
	7	Image	UVW1
	8	Image	UVW2

Table 1: Operational modes used

The first four tasks in the above list are mostly "pipeline-intrinsic", *i.e.* not expected to be user by an interactive user. All changes made to these tasks were for interface or cosmetic reasons, except for `eexmap`, where an array size had to be increased.

The Calibration Index File (CIF) used was created with a fixed processing date of 2000-12-11T00:00:00.0. The PCMS version was: 01000113/20001214.175239. There are no HK or auxiliary data plots. The products have no validation/verification flags.

2.1 EPIC products

The data contain an "unscheduled" MOS1 exposure (files `*M1U002*`). This observation was performed in low gain mode, to check the spectrum of the soft proton impinging on the detector during the high radiation interval. The images from this exposure have *not* been screened for high background.

The `hicolthresh` used in `badpixfind` to create p-n rejection masks was set to a non-nominal value of 0.003.

The p-n images suffer from a bright column and bright outer edges. These cause a number of spurious sources to be detected. Also in MOS2 a bright column is present.

The final EPIC source list is the combination of the individual EPIC maximum-likelihood source lists (cf. the `emldetect` task description) rather than the result of a simultaneous all-EPIC source detection run.

EPIC observation mosaiced images are not exposure-corrected. Background maps and three-colors EPIC images are not available.

No source-specific products have been made, because they are not considered to be reliably produced yet.

2.2 RGS products

As is presently done for any XMM exposure, a set of spectra has been made for the brightest source in the field of view of the EPIC cameras. However, owing to the dispersion of the Reflection Grating Array (RGA), the surface brightness on the RGS camera of even the brightest of the Lockman Hole sources is too small for a spectrum to be detectable. The exposure-specific detector-plane and energy-dispersion images confirm this.

2.3 OM products

The detector coordinate images are missing, as are the combined observation source list and tracking star timeseries plots (although listed in the summary).

The flatfield is derived from the CCF, not from previous in-orbit flatfield exposures.

2.4 Catalogue products

The html links to the EPIC source list do not work.

3 Functional tests of interactive tasks

All scientific products (images, spectra, light curves, filtered event lists) can be extracted by `evselect/xmmselect` on both MOS and p-n data, also if science-driven data screening criteria as described in the SAS UH are employed.

The source detection task works as well. `edetectproc` has been run on images in the 0.5-10 keV, 0.5-2 keV, and 2-10 keV energy bands. Source lists can be created for all three EPIC cameras.

4 EPIC Astrometry

In the forthcoming analysis, we have removed intervals of high radiation to increase the source detection S/N ratio, rejecting all photons with arrival time later then 32.7 ks from the start of the observation. Moreover, only MOS events with: `#XMMEA_EM` true, `PATTERN`$\leq$12 and `FLAG`=0 have been retained. Analogously, only p-n event with `#XMMEA_EP` true have been retained. The bright column in the p-n images has been removed manually, with the selection expression: `(!(DET X,DETY) IN box(7717.75,5338.75,206.25,6888.75,0))`.

In this Section, we discuss the results obtained if `edetectproc` is run with default parameter values for `ecf` and `likemin`. The effect of relaxing this constraint will be discussed in Sect. 4.4.

4.1 The background "local" method in `eboxdetect`

The local background detection method yields 33 sources for MOS1, 29 for MOS2 and 57 for p-n on the 0.5–10 keV images. Fig. 2 shows the MOS1 and PN images with sources overlayed (as obtained through the SAS `srcdisplay` task). Comparison of common sources show that 23 of the 29 MOS2 sources are found on MOS1. Out of the 33 MOS1 sources, 27 are found on the PN image as well as 25 of the 29 MOS2 sources. Visual inspection shows in addition that only a few sources (5 out of the 57 found) by PN are obviously "fake". They are all very close to a detector gap. This seems to indicate residual problems with the computation of the local background with a close empty region. Not a single fake is found by visual inspection on the MOS images.

We have looked at the quoted positions of the commonly found sources among the cameras. Fig. 3 shows a scatter plot of absolute differences between the positions of an individual source found both by MOS1 and PN versus the absolute distance to the center of the image. No correlation is found. The mean deviation is 5.2 arcsec. Fig. 4 correlates the deviations in the MOS1/p-n source positions with the number of MOS1 counts. For low number of counts there is a flat distribution centered around 5 arcsec, whereas a larger number of counts lead evidently to a better source position accuracy.

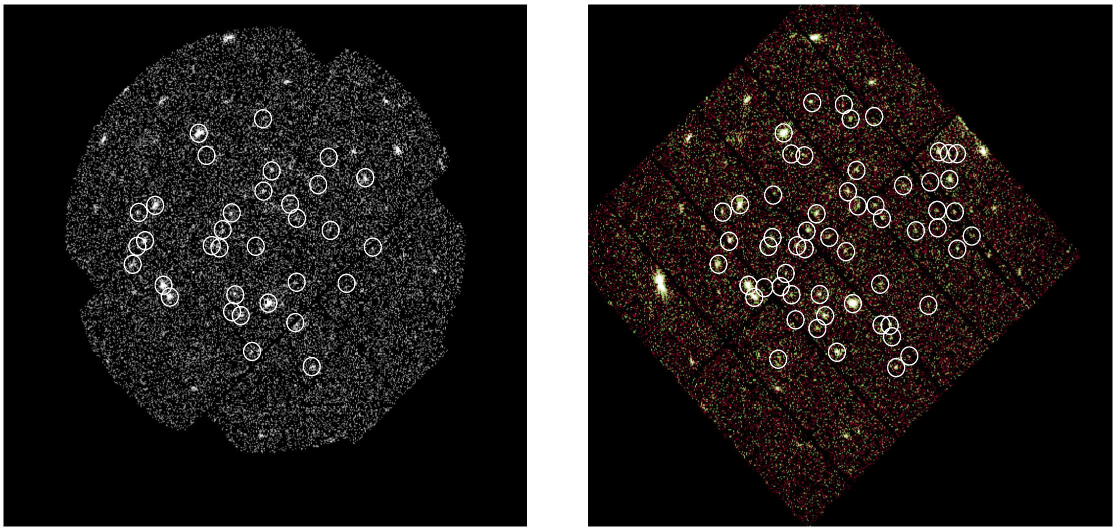

Figure 2: *Left panel*: MOS1 image in the full energy band with sources overlay *Right panel*: The same for the p-n

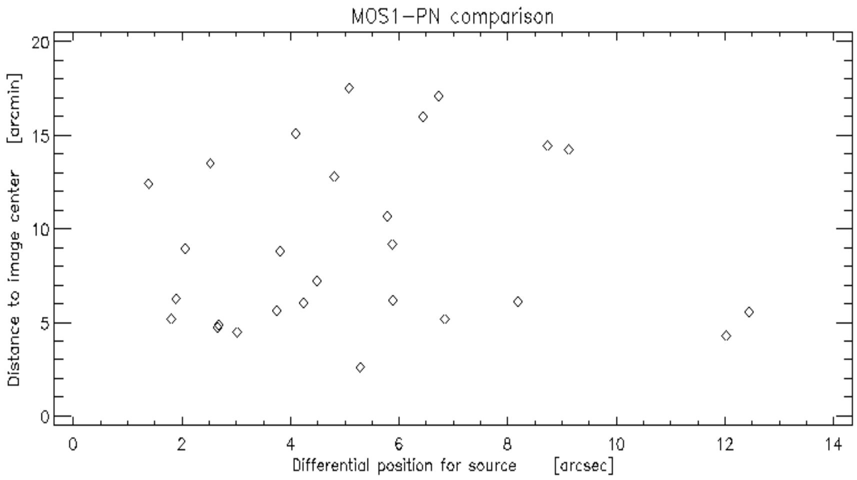

Figure 3: Distance to image center versus the MOS1/p-n position difference for sources detected in both the MOS1 and the p-n image

The uncertainties on the coordinates, as produced by the source finding algorithm, are likely to be not fully reliable yet. The combination of the uncertainties on the sky coordinates for a source detected by two instruments is generally one order of magnitude higher than the difference in position between these instruments.

4.2 The background "map method" in `eboxdetect`

Using the background map method we find 71 MOS1, 73 MOS2 and 116 PN sources. All the sources found with the local background method are found also with this method. In the PN image there are 5 "sources" on the "local" list which have not been found in the "map" list (coinciding with the 5 fake sources found by visual inspection). This is underlining the high efficiency of the source finding method. However, cross comparisons between the EPIC instruments show larger rates: only 44 out of the 71 and 73 MOS sources are "common". 14 of them have a coordinates' distance of more than 10 arcsec, suggesting that many of them are just that close by chance. We conclude that around 50% of the found sources are "fake". This is also the qualitative conclusion after visual inspection.

A comparison of the position of sources commonly found in MOS1 when `eboxdetect` is run with the "local" and "map" background estimates is shown in Fig. 5. The average source position inaccuracy is 3.9 arcsec, *i.e.* of the

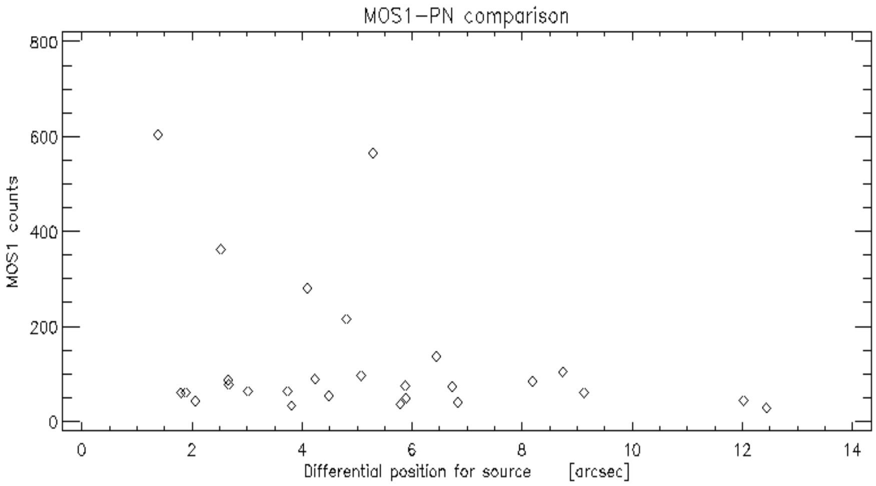

Figure 4: MOS1 source counts versus MOS1/p-n position difference for sources detected both in the MOS1 and in the p-n image

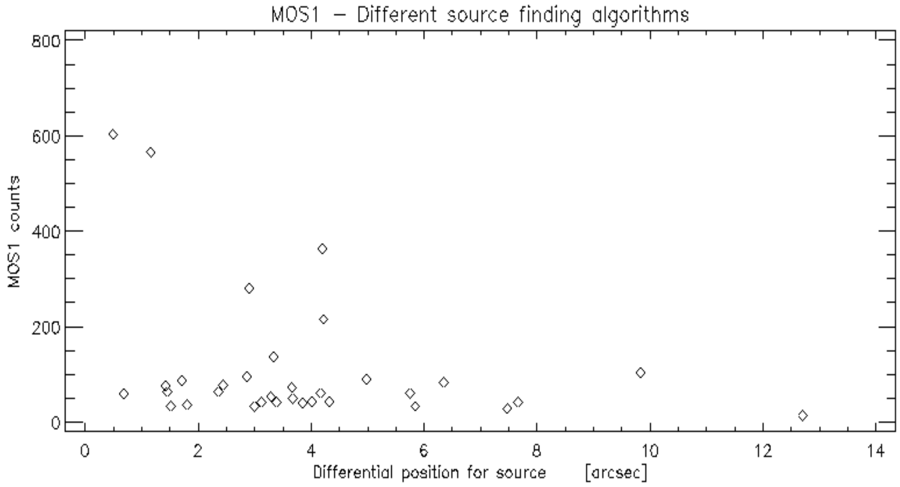

Figure 5: MOS1 source counts versus position difference for sources detected using the "local" and the "map" background algorithms

same order as the average difference between the source positions determined in the MOS1 and p-n using the same method to estimate the background. This suggests that the residual cross-calibration uncertainties between MOS(1) and p-n are within the accuracy of the source finding algorithm.

4.3 Absolute astrometry

Hasinger et al. (2001; private communication) have produced a list of sources found using the whole set of Lockman Hole XMM-Newton observations. The positions were corrected using cross identifications with optical/NIR/sub-mm, ROSAT and *Chandra* sources. A total of 127 sources was the result.

We have compared the source coordinates of Hasinger's list, with those determined by the `edetectproc` run, in order to (*semi*-independently!) check the absolute astrometry. First results suggests:

- an excellent agreement in terms of number of detected sources: 30 sources out of 33 MOS1, 26 sources out of 29 MOS2 and 48 out of 57 PN candidates, obtained with the local background mode,
- a mean distance to the "nominal position" of 5.8 arcsec for MOS1, 6.3 arcsec for MOS2 and 5.2 arcsec for PN (Fig. 6 shows the distribution),

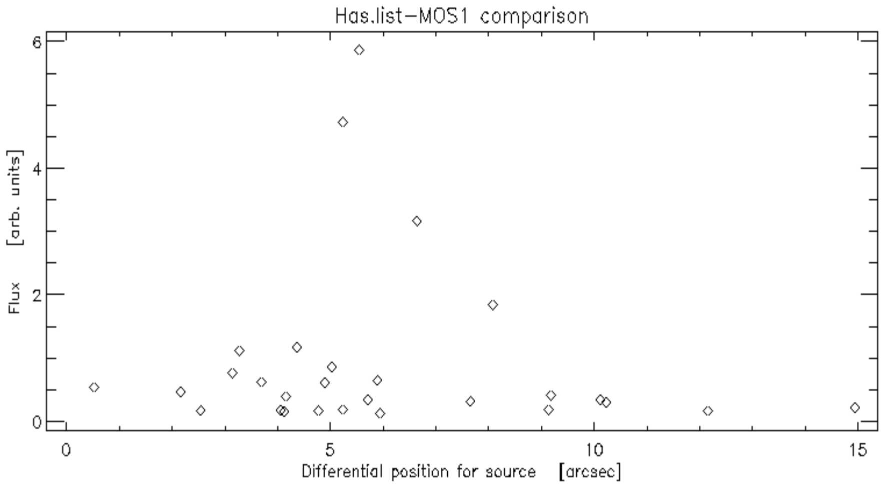

Figure 6: Source intensity versus distance between MOS1 `edetectproc`-determined (this report) and Hasinger et al. (2001) coordinates

- a confirmation of the incorrect identification by the "map" mode (*e.g.*: 49 out of 71 MOS1 "identified" sources were found in Hasinger's list).

4.4 Deviating from the default parameter values in `edetectproc`

The `edetectproc` interface allows the user to set the following numerical parameters: `ecf`, the flux to count conversion factor (in units of 10^{-11} erg cm^{-2} cts^{-1}) and `likemin`, the minimum detection likelihood for `eboxdetect`. `ecf` must be set to the correct energy correction factor in each image energy band. It must be specified in the format: `''ecf1, ecf2, ... ecfn''`, where n is the number of input images. `likemin` is defined as $-\ln(p)$, where p is the probability of Poissonian random fluctuations of the counts in the detection cell, which would have resulted in at least the observed number of source counts. `likemin=15` (the default value for `edetectproc`) is a conservative choice, aiming at detecting only safely true sources. Lower values ($\gtrsim 8$) can maximize the detection sensitivity, at a cost of a larger extraction time and - of course - of a larger number of spurious detection. The user is urged to apply her/his own scientific judgment to the results.

It is noticeable that in both images of Fig. 2 the detection is limited to the (more or less) central 80% region of the field of view. When `emask` is run through `edetectproc`, it retains only those parts of the image, where the exposure is higher than 50% of the on-axis value (cf. Fig. 7, left panel). This is set by the parameter `threshold1` in `emask`. Relaxing the value of this parameter (to, *e.g.*, 0.05) yields a much wider detector mask (cf. Fig. 7, right panel; MOS2 and p-n show similar behavior). This parameter cannot be set through the `eboxdetect` interface. The user, willing to modify this parameter, must run the source detection chain task-by-task, following the `edetectproc` task description.

5 Robustness of the EPIC source count determination

In Fig. 8, we show the correlation between the source counts determined by `eboxdetect` (map mode) and the integral of the counts in the source spectrum, extracted with `evselect`. The source extraction region is a 22" box, centered on the best-fit position (as determined by `eboxdetect` run in "local" mode). The plot includes the 22 brightest sources detected in the MOS 0.5–10 keV band.

No correction for photon loss due to the Point Spread Function (PSF) is taken into account in the counts measured from the `evselect`-produced spectra (the PSF-correction within SAS is performed at the response generation level). We therefore overlap to the plots of Fig. 8 the loci corresponding to the encircled energy fraction at 0.5 (55%) and 10 keV (45%), according to the XMM-Newton User Handbook. The counts measured via the extraction of scientific products are $\simeq$10% higher than those measured by `eboxdetect` for sources with about 50 counts. The difference decreases for brighter sources. It is difficult to say at this stage which of the two methods provides the most accurate results. The former is affected by missing PSF fraction; moreover, the assumed fixed extraction radius means that

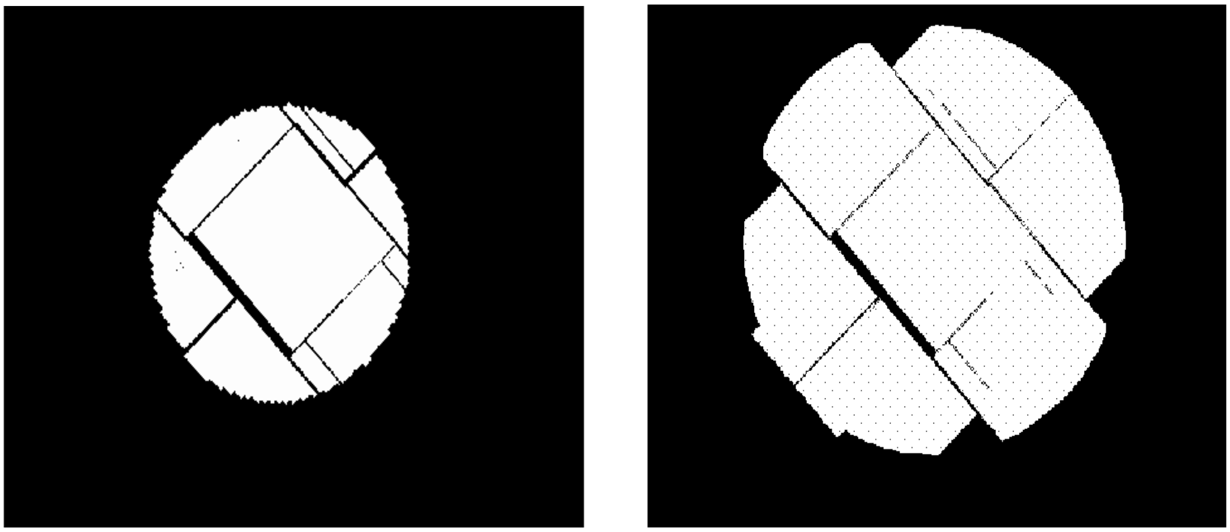

Figure 7: Sensitivity mask for MOS1 as produced by `edetectproc` with: `threshold1=0.5` (*left panel*), and `threshold1=0.05` (*right panel*) in `emask`

this missing fraction is a function of the off-axis angle. The latter is likely to be affected by high systematic errors in the background estimation when the "map" mode is used. However, regardless of the details, the above results suggest that the counts are likely to suffer systematic errors $\lesssim 10\%$ in sources brighter than $\simeq$50 counts. For sources weaker than $\simeq$30 counts, systematics of the order up to 50% are possible.

The agreement between the count rate determined by `eboxdetect` (in "map mode") and `emldetect` is within a few percent (see Fig. 9).

6 OM astrometry

A quick comparison with coordinates obtained from CDS-POSSI/E/DSS1 digital sky survey (without PSF fitting) gives consistent coordinates within 3-4 arcsec over the full OM FOV, in all filters, both for 2×2 binned images and full resolution central windows.

Source detection is made difficult by the presence of straylight artifacts. No detailed analysis has been performed. However, a quick analysis shows that good detections rates are achieved. There are discrepancies of a few tenths of magnitude when comparing results from big 2×2 binned windows and the central high resolution window.

Acknowledgments

We acknowledge useful comments from H.Brunner - author of the source detection SAS tasks - and F.Jansen.

References

M.Dahlem, *XMM Users' Handbook*, XMM-PS-GM-14, available at:
`http://xmm.vilspa.esa.es/users/uhb_top.html`
G.Hasinger et al., 2001, A&A, 365, L45

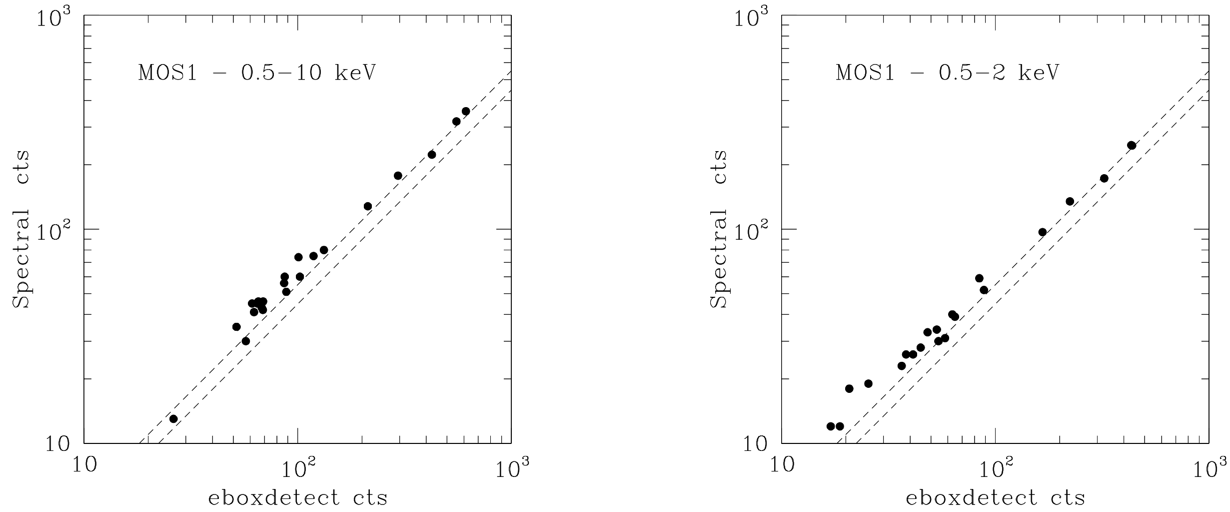

Figure 8: Correlation between the sources count determined by `eboxdetect` (in "map mode") and `evselect`- extracted spectra in the MOS whole energy band (0.5–10 keV; *left panel* and soft band (0.5–2 keV; *right panel*). The *dashed lines* mark the encircled energy fraction at 0.5 (*higher*) and 10 keV (*lower*)

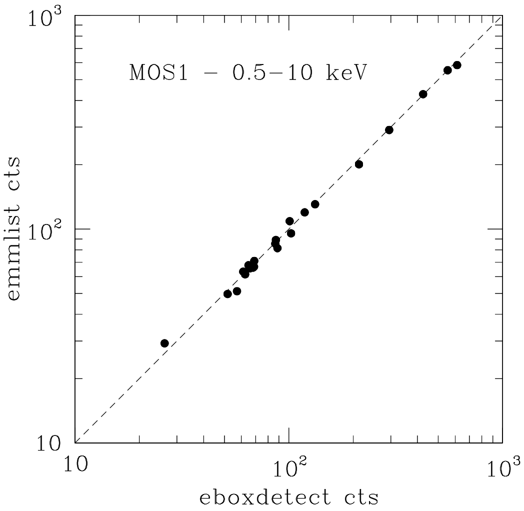

Figure 9: Correlation between the sources count determined by `eboxdetect` (in "map mode") and `emldetect` in the MOS whole energy band (0.5–10 keV)